Experimental investigation and probabilistic modeling of shear resistance and stress-volumetric unit deformation behaviors of sands having different mineralogies

Dr. Seda ÇELLEK

Abstract

This study aimed to examine the shear strength and stress-unit deformation behaviors of dry sands under static loads with the help of shear box experiments. For that purpose, sea sand taken from Trabzon, Sinop, and Zonguldak Provinces and river sand taken from Aydın Çine District were used. We attempted to evaluate geological and mineralogical properties of natural sand of different origins.

For the classification of samples, specific gravity, sieve analysis, and maximum and minimum dry density tests were performed in the first stage. During the shear box experiments, the samples prepared at different empirical (varying) compaction varying between 45% and 85% were consolidated under vertical stresses varying between 30 and 400 kPa and then loaded up to failure. On the basis of the test results, Mohr-Coulomb failure parameters were determined according to relative compaction and effective stress. Semi-empirical relationships specific to the sands were developed due to relative compaction and effective stress in accordance with the principles of soil mechanics, as well as critical conditions for determination of Mohr-Coulomb strength parameters and volumetric unit deformation and bounded module values. The maximum likelihood method was used to determine the model parameters of the equations.

In addition, physical properties were determined by experiments, and static parameters of sand samples were obtained. For this purpose, the material properties, stress-strain properties, and grain crush pressures of sand samples were calculated. A probabilistic model has been introduced by using soil parameters obtained from experiments.

Keywords: sand, mineralogy, shear box, strength, shear resistance, shear stress, shear unit deformation, maximum likelihood, limited module, volumetric unit deformation

1. Introduction

Soils are formed by geological processes, so the engineering behavior of each soil varies. For example, two different sand samples with the same mineralogy or granulometry curve may exhibit different compressive properties under the same stress. The void distributions of the soil and the orientation of the particles vary according to the direction and amount of stress applied. The grains forming the natural soils are formed by fragmentation of rocks into small pieces as a result of mechanical and chemical weathering. Because the rocks forming the grains have very different mineralogical structures, and because the factors leading to the grain segregation are different, there are different sizes and shapes of grains found in natural soils. These minerals, some of which have a fragile and planar structure, are divided into very small pieces and form fine grains (Özaydın, 2000). Different sizes and shapes of the grains in the ground also affect engineering behaviors. There is a close relationship between the texture of the soils and their engineering behavior. Soil structure affects the stress and deformation behavior of the soil, as well as the peak strength value. Soils can exhibit different stress-strain behaviors at the same void ratio due to structural differences and intrinsic anisotropy (Sezen, 2003). The decrease in the size of the grains of the soils increases the flatness of the grains. With the increasing flatness

of the grains, surface-to-surface interaction between the grains is more effective, even if the grains are randomly aligned. Permanent (residual) slip resistance decreases as the number of flat-shaped grains in the soils increases (Bayın, 2011). The shear resistance of the soils is dependent on the void ratio (e), the type of the soil, the geologic history, the stresses that were applied (σ), and the texture of the soil. Those soil properties are interdependent, but the mathematics is defined for convenience relative to strength, cohesion (c), and internal friction angle (ϕ) (Özaydın, 2000). Compaction of the ground is one of the most important factors that determine the behavior of non-cohesive soils under repetitive loads, as in the case of static loading. It is common practice to describe the structural behavior of non-cohesion-based soils on the basis of relative compaction (Şener, 2009). The strength and stiffness of coarse-grained soils are known to vary with respect to mineralogical factors, as well as the relative distance to the critical condition curve (Duncan, 1980; Jefferies and Been, 2006). In simple terms, there are significant differences in the strength and tensile-unit deformation behavior of the same sand samples with different void ratios and effective stress conditions. Therefore, it is known that the cohesion (c) and shear resistance angle (ϕ) values with Mohr-Coulomb strength parameters are not a fixed (non-variable) parameter set--depending on the material, but also on the relative compaction of the material and the effective stress conditions (De Mello, 1971; Sowers, 1979; Stroud, 1989). Similarly, it is also stated in the literature that the stiffness modulus for coarse-grained materials will vary with the relative stiffness of the material and the effective stress conditions (Duncan, 1980). Because sand behaves very differently from clay, modeling efforts on it is generally much difficult. For example, it is well known that, unlike loose sand, tight sand expands under shear. The same sand tends to behave like different materials under different conditions of density and pressure. The fact is that sand behavior depends on the level of pressure applied to it and on its firmness. As the sand fragments break, the number of particles increases. Of course, resistance to breakage depends on the mineral composition of the sand (Ling and Yang, 2006). Some changes occur in the structure of the soils during compression and volume change. A reorganization of the structures of the soils takes place as a result of compaction, as the size of the grains may change and shape changes may occur. Such shape changes may occur in the form of permanent (plastic or viscous) or elastic deformations, depending on the duration of the compression and the stresses that cause the compression. However, to distinguish those factors, micro-behavior must be defined (Yüksel, 2007). Shear box experiments were performed in this study for the determination of the Mohr-Coulomb strength parameters and shear moduli of four sand species with different mineralogical properties under different relative stress and effective stress conditions. Based on the experimental results, semi-empirical probabilistic relationships have been developed for the determination of the strength parameters and shear moduli of four different sands.

2. Sand Samples

The natural sands tested were sampled from Sinop-Sarıkum ($42^0$01'29"N, $34^0$55’22"E), Trabzon-Akçakale ($41^0$04’48"N, $39^0$30’3’"E), Zonguldak-İnkumu Beach ($41^0$37’54"N, $32^0$20’02"E), and Aydın-Çine Menderes River bed sites ($37^0$36’42"N, $28^0$03’41"E). Sinop Sand (SNP) was obtained from units belonging to the Sarıkum Formation, which is composed of fine-grained sandstone, mudstone, conglomerate, and limestone. Zonguldak (ZNG) sand is derived from the Yılanlı Formation, and the formation is composed of limestone, dolomitic limestone, and dolomite and cherty limestone alternations. Trabzon sand (TRB) is from the Kabaköy Formation. The formation consists of sandstone/sandy limestone/tuff intercalations,

andesite lava, basalt lava, and pyroclastics. On the other hand, Çine Kumu is a member of the Menderes Massif. The unit consists of augen gneisses of granitic origin, white-to-gray colored hard-textured quartz schist, and decomposed metamorphics.

Figure 1 presents the grain shapes obtained by scanning electron microscopy (SEM) analysis of the sands.

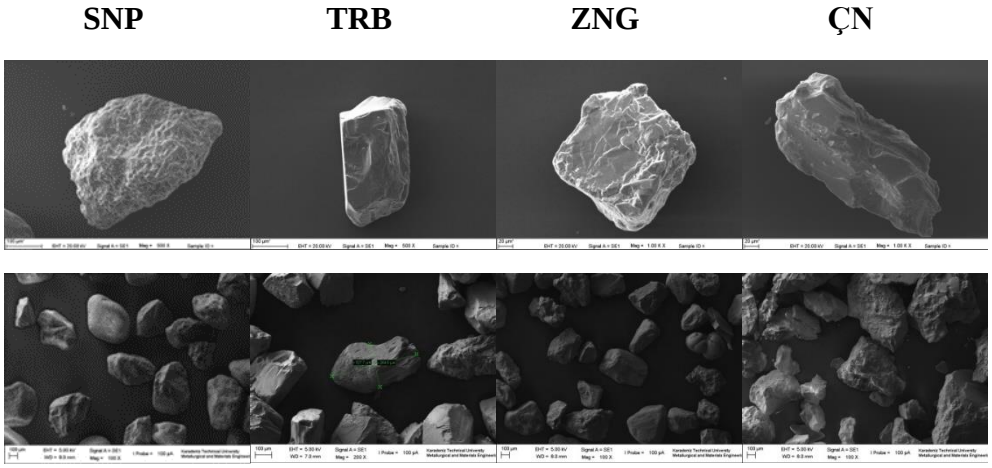

Figure 1. Scanning Electron Microscopy (SEM) images of sands used in the study

As can be seen from the figures, SNP sand consists of round grains, and TRB sand contains more angular grains. ZNG sand has semi-angular and rounded grains. ÇN sand is generally composed of semi-angular grains. Due to the common origin of SNP and ZNG sands in which occurred in sedimentary basins, their mineralogical properties are similar. TRB and ÇN sands are of igneous and metamorphic origin, respectively. Analyses were carried out with illuminated and binocular optical microscopes for the determination of the mineralogical structures of the sands. The X-ray diffraction method (XRD) was used to determine the mineral contents of sand samples, and the results are shown in Figure 2 and Table 1. Quartz and anorthite were found in SNP, ZNG, and ÇN sands, whereas muscovite was observed only in EBA sand. TRB sand has different mineralogical characteristics from the other three types of sand, with a mineralogical composition of augite, hedenbergite, diopside and fayalite.

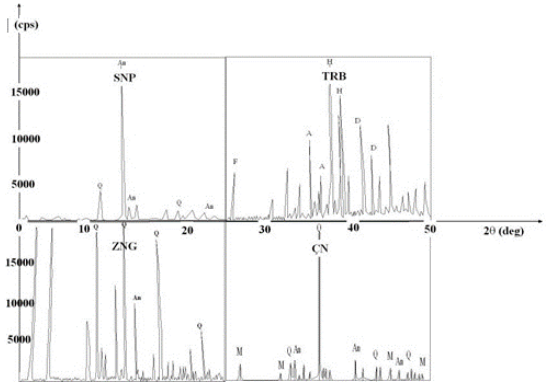

Q: Quartz, An: Anorthite, A: Anorthoclase, F: Fayalite, H: Hedenbergite, D: Diopside, M: Muscovite

Figure 2. X-ray diffraction (XRD) analysis of sand

Table 1. Mineralogical properties of sands used in the study

Mineral Chemical Formula	SNP%	TRB%	ZNG%	ÇN%
Quartz SiO_2	57	-	80	48
Anorthite $CaAl_2Si_2O_8$	43	-	20	32
Augite $Ca(Mg,Fe)\ Si_2O_6$	-	53		
Diopside $(Mg,Al)(Si,Al)_2O_6$	-	20		
Hedenbergite $CaFe^{+2}Si_2O_6$	-	20		
Fayalite $Fe^{+2}SiO_4$	-	7		
Muscovite $KAl_2Si_3AlO_{10}(OH)_2$	-			20
Total	100	100	100	100

The defining properties of the samples and grain sizes were determined by laboratory experiments (Figure 3).

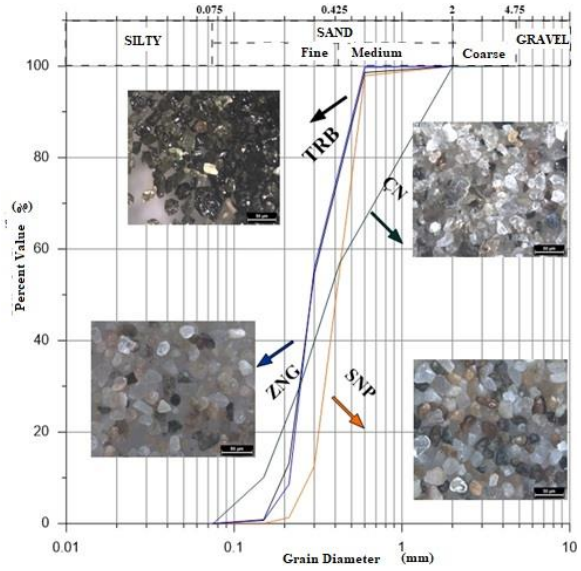

Figure 3. Grain distribution curves of sand samples used in the experiment

The minimum and maximum void ratios and dry unit weight values were obtained in order to prepare the sand samples at the desired compaction. Table 2 shows that SNP, ZNG, and ÇN sands have similar mineralogies and specific gravities. Due to its mineralogical structure of iron and magnesium, TRB has a higher specific gravity than the other three types of sand. The fine-grained constituents of the sands, which were classified as poorly graded (SP) according to the Unified Soil Classification System (ASTM D-2487), were washed away.

Table 2. Grain distribution properties of the sands used in the study

	SNP	TRB	ZNG	ÇN
Grain structure	Rounded	Angular	Semi-angular–Rounded	Semi-angular
$Sand_{fine}$ (%)	88	94	94	56

$Sand_{medium}$ (%)	12	06	06	46
Specific Gravity, G_s	2.74	3.44	2.75	2.75
Minimum Void Ratio, e_{min}	0.55	0.66	0.60	0.60
Maximum Void Ratio, e_{max}	0.85	0.91	0.85	0.93

3. **Shear Box Experiments**

Direct shear tests were performed in accordance with ASTM Standard D-3080-98 to determine the shear strengths of the sands. Dry sand samples with a relative densities ranging from 45% to 85% were consolidated under vertical effective stresses in the range of 30–400 kPa and subjected to shear box tests to determine the deformation/shear stress behaviors and strengths of the samples. Vertical effective stress and relative compaction (D_R) distributions of the prepared samples are shown in Figure 4.

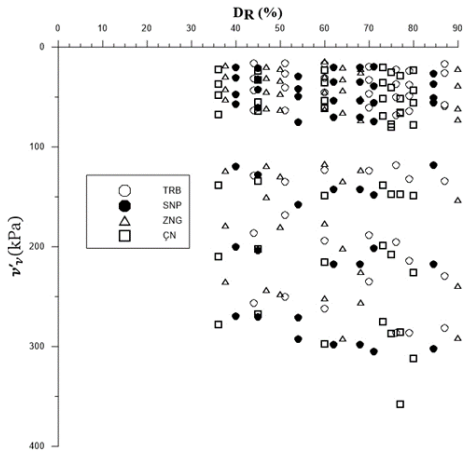

Figure 4. Vertical effective stress and relative compaction distributions of prepared sand samples

Figure 5 shows the shear stress and volumetric unit deformation graphs that were drawn according to the results of the unstabilized, non-drained shear box test results for the four sand types. The cohesion values measured during the experiments varied in a very low range of 0–2 kPa, as expected from the dry sands. The maximum shear resistance angle value was defined as the shear stress angle value at the time the shear stress/vertical effective stress value reached the maximum during the experiment and was calculated by assuming that the cohesion was zero. In the experiments, there are very significant differences in shear modulus under different effective and shear stresses in sand samples starting with similar empirical compaction. The secant shift moduli, G_{25}, G_{50}, and G_{75}, and the secant shift modulus at the time of defeat are the shear stresses equal to 25, 50, 75, and 100 per cent of the shear strength $_{emax}$, so that the shear stress coefficients are 4, 2, 1.5, and 10, respectively. G_{100} values are also summarized in Table 3 for all types of sand.

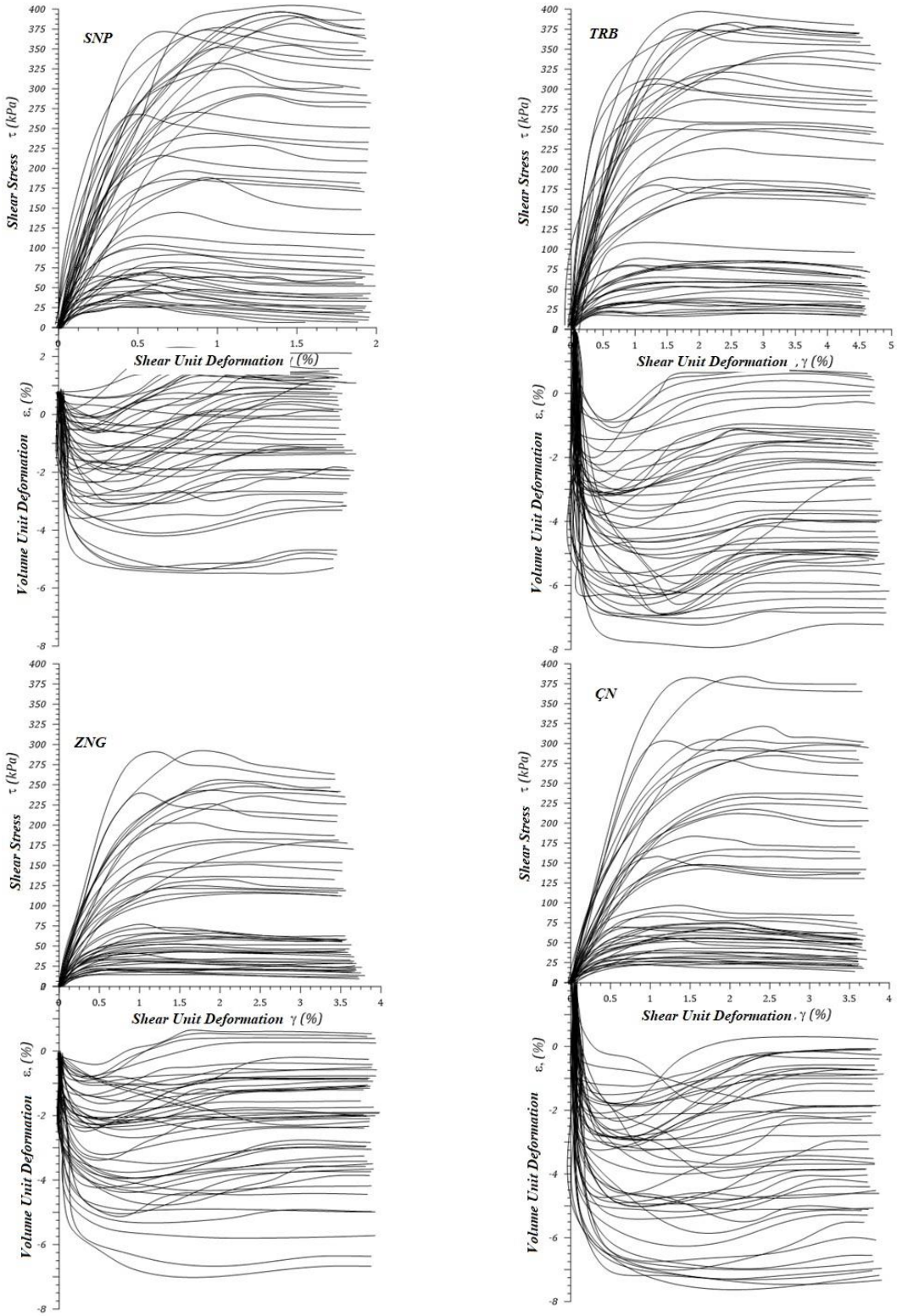

Figure 5. Shear stress and volumetric unit deformation graphs of four sands

Table 3. G values calculated by shear box experiments for four sands

SNP				TRB				ZNG				ÇN			
G_{25}	G_{50}	G_{75}	G_{100}	G_{25}	G_{50}	G_{75}	G_{100}	G_{25}	G_{50}	G_{75}	G_{100}	G_{25}	G_{50}	G_{75}	G_{100}

136	88	36	19	113	74	37	6	200	83	32	13	127	95	46	20
166	88	56	28	204	120	43	20	181	98	75	23	167	108	59	25
195	146	110	46	225	130	68	28	195	150	107	30	205	130	88	31
122	107	88	45	263	134	88	33	205	94	77	32	291	160	103	41
213	163	116	65	225	208	124	62	310	265	178	83	317	277	190	90
305	265	201	117	275	247	193	93	337	255	187	83	261	252	195	103
281	240	196	142	506	350	243	108	459	338	230	104	312	347	220	105
147	98	54	16	200	167	72	14	200	147	64	14	142	73	43	16
155	73	45	25	156	80	42	18	200	146	77	19	132	71	46	16
193	61	50	30	215	88	57	30	195	120	69	28	224	104	84	30
224	117	95	44	349	178	78	33	173	142	103	38	170	118	87	35
210	200	163	84	233	231	153	69	204	203	145	50	370	232	169	96
198	188	191	134	412	306	230	102	400	275	207	67	296	269	207	113
316	314	243	165	479	365	278	117	436	344	273	154	430	325	246	117
98	92	91	44	200	157	54	12	250	192	92	23	147	120	58	22
118	124	102	39	185	91	45	21	250	146	75	33	181	146	80	34
216	180	155	29	350	250	114	24	229	136	82	35	130	110	82	50
195	180	175	105	323	186	115	43	273	172	115	52	214	113	85	60
245	290	260	106	370	280	163	70	242	194	158	76	203	201	173	146
320	310	300	196	317	336	241	113	186	150	117	64	208	213	190	211
340	316	273	131	290	318	250	100	319	368	256	118	277	258	225	289
148	96	53	29	200	125	61	17	200	128	43	11	147	110	64	24
207	143	63	39	186	145	86	37	250	85	52	20	65	57	46	30
256	123	105	60	225	147	95	26	247	126	69	28	322	243	175	80
285	163	109	51	225	179	95	33	225	206	157	52	181	139	122	61
265	242	179	95	224	228	175	85	243	200	155	71	339	256	201	90
278	272	226	110	269	259	211	86	436	364	255	108	229	217	205	121
370	332	263	138	339	289	238	99	402	337	255	121	380	343	273	168
108	83	61	23	200	109	71	24	128	89	65	16	118	62	32	13
245	172	110	41	300	168	95	30	250	152	103	36	350	293	112	31
244	159	99	49	245	140	80	31	224	180	134	45	233	112	67	32
292	221	190	73	294	196	165	67	156	125	100	49	331	188	107	47
244	226	201	123	211	274	217	94	282	237	211	131	218	207	168	91

291	291	239	151	437	355	277	119	290	285	255	151	257	234	184	103
377	361	317	211	333	343	297	169	354	402	333	184	427	344	285	136
177	128	105	35	147	96	97	24	200	98	55	19	148	107	93	29
284	194	150	41	196	130	100	27	250	213	35	8	249	210	149	51
285	221	146	61	245	145	110	46	225	125	97	45	284	216	189	114
342	257	205	89	264	182	160	63	225	152	140	61	197	194	180	95
400	353	269	116	260	254	211	88	369	252	187	85	285	280	270	166
375	322	278	172	307	310	265	126	300	278	230	137	356	408	395	273
440	387	292	182	307	315	295	168	436	355	282	131	471	447	405	264
167	134	98	38	300	250	131	26	160	140	116	87	138	83	48	18
143	143	125	75	142	99	78	32	105	84	77	44	235	176	120	45
392	297	281	85	160	150	140	80	180	154	131	80	244	122	101	49
161	149	119	62	297	285	223	90	209	194	162	77	303	228	163	73
208	199	165	102	301	296	262	152	226	238	228	154	316	253	204	99
549	490	461	272	568	431	395	242	414	384	379	266	422	320	235	139
620	512	467	287	326	356	334	226	442	453	420	292	430	343	279	160

4. Formulas of Semi-empirical Probability and Slip Resistance.

In accordance with the behavior of critical soil mechanics, the maximum effective shear resistance angle, ϕ, for sands can be modeled as shown in Equation 1 with normal effective stress ( ) and relatively firm stress (D_R) (Bolton, 1986).

$$\phi = D_R * \theta_1 + \theta_2 - \theta_3 \ln\left(\frac{\sigma'}{Pa}\right) \quad [1]$$

In Equation 1, atmospheric pressure, P_a, and model coefficients, θ, are calculated by the maximum likelihood method. For the slip resistance angle, the limit equilibrium model, g($\phi, D_R, \sigma'\theta,$), is written as the error value, as shown in Equation 2.

$$g(\phi) = \phi model - \phi \text{measured} = D_R * \theta_1 + \theta_2 - \theta_3 \ln\left(\frac{\sigma'}{Pa}\right) - \phi \text{measured} + \text{e} \quad [2]$$

In the equation, $\phi'_{\text{model}} - \phi'_{\text{measured}}$, with ϵ corresponding to the error term in the equation, is used to model the effects of the selected function in the scope of the limit equilibrium model to the effects of other input parameters (e.g., grain shape, mineralogical factors, compressibility) that have an effect on the slip resistance angle and are not included in the model. To produce the correct estimates (mean error zero), the error term is ϵ, the mean is zero, and the standard deviation is σ_ϵ. The normal distribution, in terms of ease of calculation, is followed by the likelihood function given in Equation 3.

$$L(\boldsymbol{\theta},\sigma_\varepsilon)=\prod_{i=1}^{196}P\left[g(\phi_i,\varepsilon_i,\boldsymbol{\theta})=0\right]=\prod_{i=1}^{n}\varphi\left[\frac{\varepsilon_i}{\sigma_\varepsilon}\right] \qquad [3]$$

$\varphi[\cdot]$ is the standard normal probability function, which is the function of model parameters $\boldsymbol{\theta}$ and mode error σ_ε which is the standard deviation value. In the writing of equation 3, it was assumed that the results of the experiments were statistically independent. Model parameters that maximize the likelihood equation given in Equation 3 within the maximum likelihood method are calculated as presented in Table 4.

Table 4. Slip resistance angle model parameters

	SNP		TRB		ZNG		ÇN		All Sands	
Model Coefficient	ϕ_{max}	$\phi_{res.}$	ϕ_{max}	$\phi_{res.}$	ϕ_{max}	$\phi_{res.}$	ϕ_{max}	$\phi_{res.}$	ϕ_{max}	$\phi_{res.}$
θ_1	3.65	0.00	7.10	0.00	11.13	0.00	7.10	0.00	5.06	0.00
θ_2	32.70	33.55	30.90	31.88	23.28	30.84	30.90	35.09	30.83	32.72
θ_3	0.56	0.00	1.20	0.00	0.94	0.00	1.20	0.00	0.71	0.00
$\sigma_{\phi'}$	3.14	3.66	2.60	2.55	2.65	3.33	2.60	2.67	3.40	3.32

The effective shear resistance angle relationship is shown in Figure 6 for the test data. In addition, to determine whether the models produce a systematic error, the variation of the error term, which is defined as the difference between the estimated values and the measured values, is presented in Figure 6. The error term does not show a correlation with the model input parameters Dr and Sigma and the mean error in the zero order shows the success of the model in generating an unbiased estimate. The magnitude of the standard deviation of the model error term indicates the possible uncertainty in the calculation of the shear resistance angle on the basis of only relative compaction and effective stress.

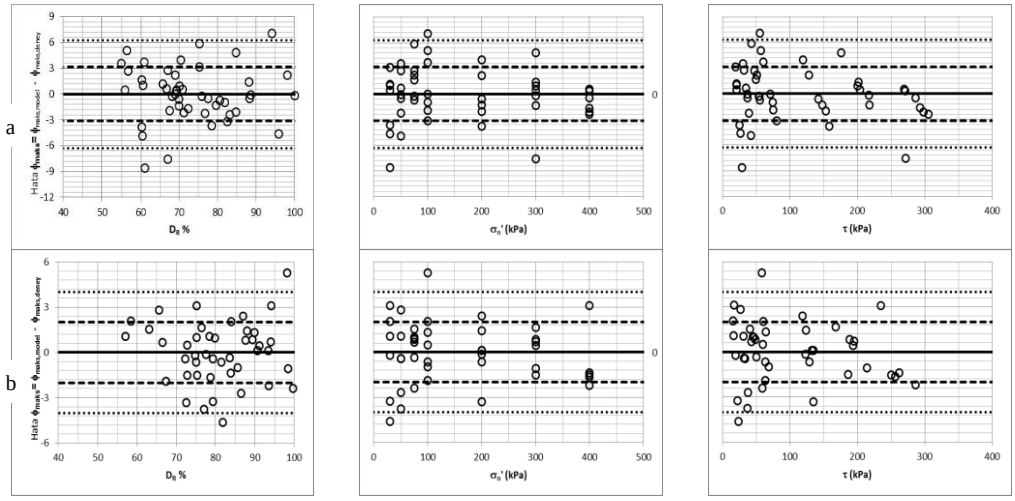

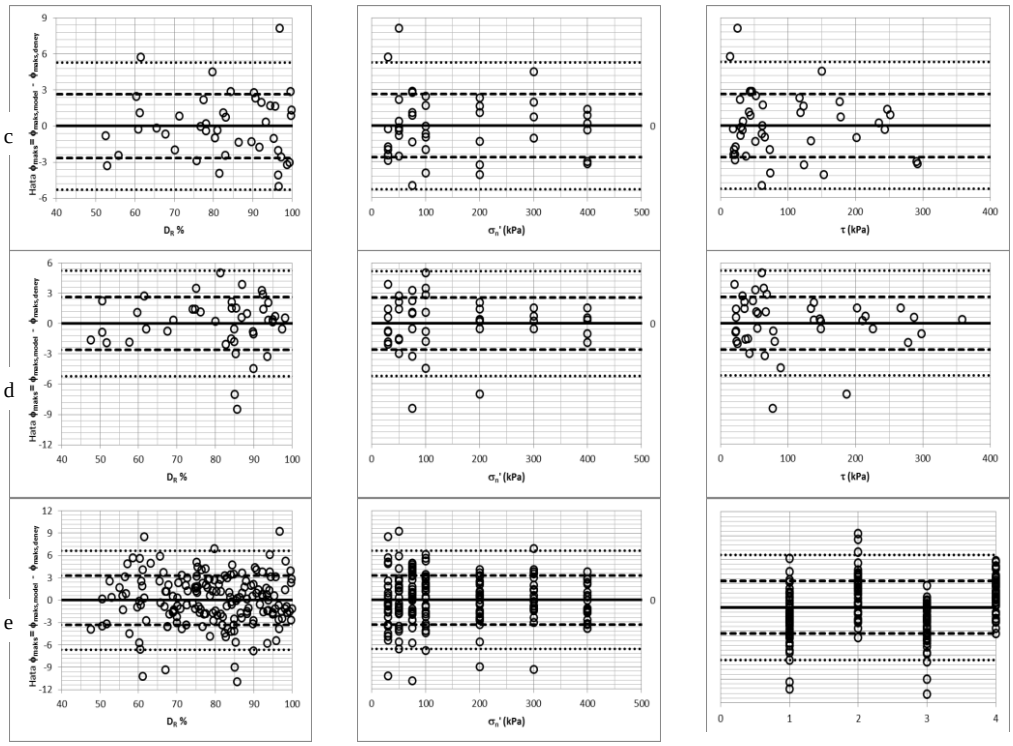

Figure 6. ϵ_i for sands, change of error term with relative compaction and effective stress, a) SNP, b) TRB, c) ZNG, d) CN, e) All sands

The median (mean) $\pm$ σ_ϵ in estimates of the developed model are shown in Figure 7 as a function of effective stress and empirical compaction.

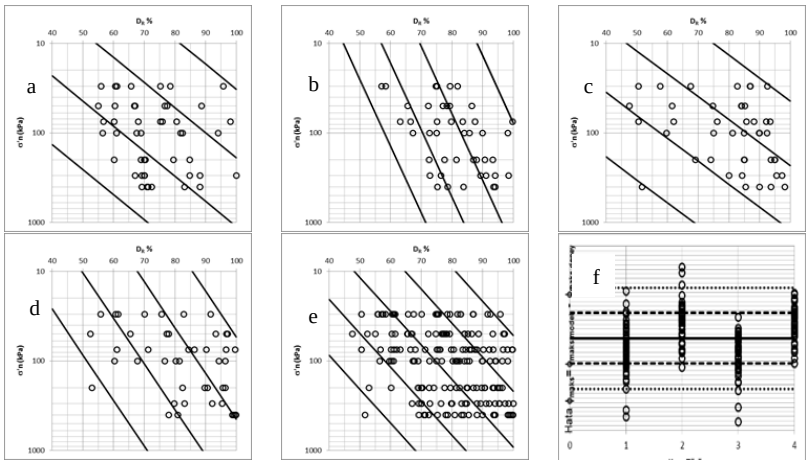

Figure 7. Mean v± model estimation for sands, a) SNP, b) TRB, c) ZNG, d) ÇN, e) All Sands f) Distribution of all sands according to model

5. Semi-empirical Probabilistic Slip Modulus Formulas

The equation can be modeled as shown in Equation 4 with the effective stress and the relative compaction of the G modulus on the basis of the existing shear modulus correlations in the literature (Duncan, 1980; Bolton, 1986).

$$G_{estimation} = \theta_1 * \left(\frac{Dr}{100}\right)^{\theta_2} * \left(\frac{\sigma}{Pa}\right)^{\theta_3} \quad [4]$$

As discussed previously, the limit equilibrium model and likelihood equations have been developed in similar fashion to Equations 2 and 3. Again, using the maximum likelihood method, the model parameters and the standard deviation of the error term are calculated as shown in Table 5.

Table 5. Slip modulus probabilistic model parameters

Model Coefficient	SNP				TRB			
	G_{25}	G_{50}	G_{75}	G_{100}	G_{25}	G_{50}	G_{75}	G_{100}
θ_1	293.74	234.09	190.03	92.07	251.98	212.94	167.65	68.67
θ_1	0.85	0.94	1.14	1.17	0.04	0.71	1.60	1.97
θ_1	0.29	0.41	0.50	0.66	0.25	0.38	0.49	0.70
σ_G	0.24	0.25	0.30	0.24	0.23	0.23	0.23	0.23
Model Coefficient	ÇN				ZNG			
	G_{25}	G_{50}	G_{75}	G_{100}	G_{25}	G_{50}	G_{75}	G_{100}
θ_1	234.92	180.35	136.57	68.61	229.34	182.47	127.48	62.94
θ_1	0.21	0.35	0.66	0.87	-0.16	0.21	0.38	1.15
θ_1	0.32	0.45	0.56	0.75	0.29	0.41	0.57	0.67
σ_G	0.28	0.28	0.27	0.30	0.22	0.25	0.28	0.40
Model Coefficient	ALL SANDS							
	G_{25}	G_{50}	G_{75}	G_{100}	G_{25}	G_{50}	G_{75}	G_{100}
θ_1	249.23	196.14	145.62	66.83	0.25	0.48	0.73	0.95
θ_1	0.28	0.41	0.54	0.72	σ_G0.25	σ_G0.26	σ_G0.29	σ_G0.35

To determine whether the developed models are no longer producing residual errors, the error term defined as the difference between the calculated values and the measured value is presented in Figure 8, with relative compaction and effective stress. The error term does not

show a correlation with the model input parameters D_R and Sigma or with the average error in the zero order; the model achieves the success of generating an unbiased estimate. The magnitude of the standard deviation of the model error term indicates the uncertainty in the calculation of the shear resistance angle.

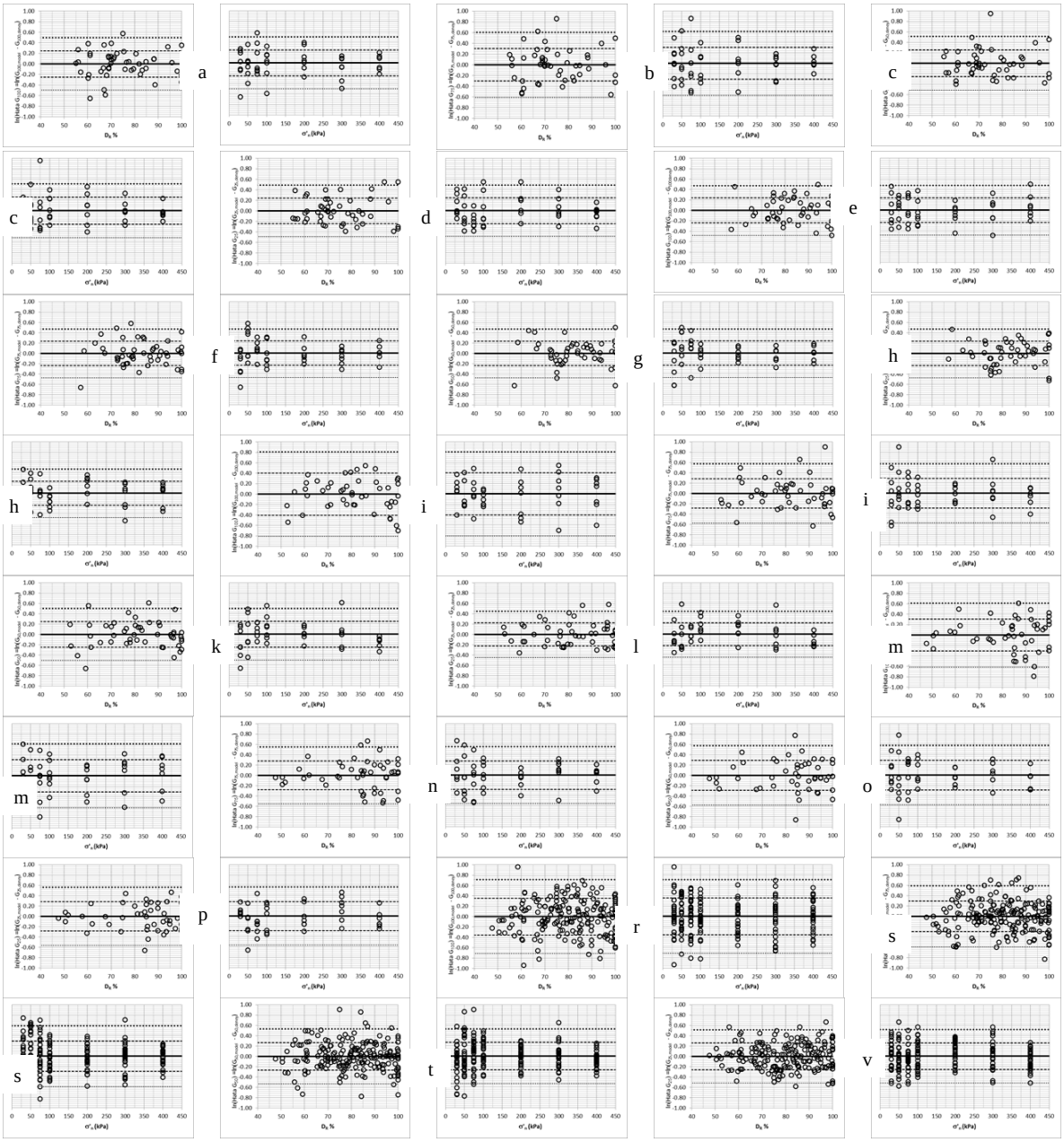

Figure 8. Relative compaction and effective stress change for sands

a) SNP sand for (G_{100}), **b)** SNP sand for (G_{75}), **c)** SNP sand for (G_{50}), **d)** SNP sand for (G_{25}), **e)** TRB sand for (G_{100}), **f)** TRB sand for (G_{75}), **g)** TRB sand for (G_{50}), **h)** TRB sand for (G_{25}), **i)** ZNG sand for (G_{100}), **j)** ZNG sand for (G_{75}), **k)** ZNG sand for (G_{50}), **l)** ZNG sand for (G_{25}), **m)** ÇN sand for (G_{100}), **n)** ÇN sand for (G_{75}), **o)** ÇN sand for (G_{50}), **p)** ÇN sand for (G_{25}), **r)** All sands for (G_{100}) error, **s)** All sands (G_{75}), **t)** All sands for (G_{50}), **v)** Alteration of error term for all sands (G_{25}) by relative strain, effective stress and sand type

The median (average) ± σ_ϵ estimates of the developed model are shown in Figure 9 as a function of effective stress and empirical compaction.

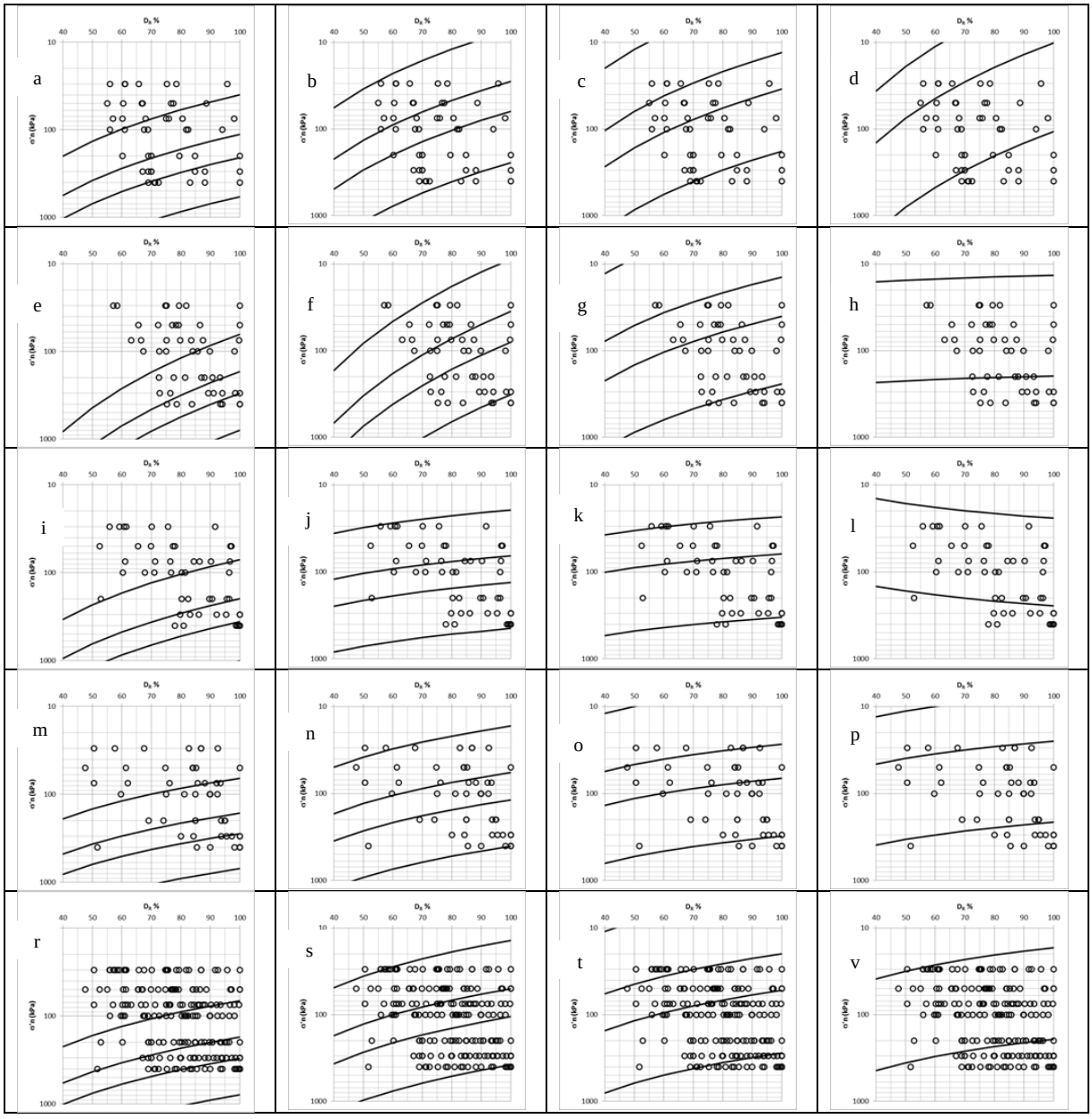

Figure 9. a) SNP sand for (G_{100}), **b)** SNP sand for (G_{75}), **c)** SNP sand for (G_{50}), **d)** SNP sand for (G_{25}), **e)** TRB sand for (G_{100}), **f)** TRB sand for (G_{75}), **g)** TRB sand for (G_{50}), **h)** TRB sand for (G_{25}), **i)** ZNG sand for (G_{100})**, j)** ZNG sand for (G_{75})**, k)** ZNG sand for (G_{50}), **l)** ZNG sand for (G_{25}), **m)** ÇN sand for (G_{100})**, n)** ÇN sand for (G_{75}), **o)** ÇN sand for (G_{50}), **p)** ÇN sand for (G_{25}), **r)** All sands for (G_{100}), **s)** All sands for (G_{75}), **t)** All sands for (G_{50}), **v)** All sands for (G_{25}), mean ±ν mode prediction

6. **Results and Discussions**

The Mohr-Coulomb deflection model internal friction angle and the effect of shear modulus with relatively tight strain and stress-strain conditions on sandy soils were investigated in this study by using the shear box experiment results. Different sand samples taken from Sinop

(SNP), Trabzon (TRB), Zonguldak (ZNG), and Çine (ÇN) were tested in the laboratory, and the behaviors of geologically different sands were compared. It was determined that the sands used in the study consist of fine and medium grains. It was determined as a result of the experiments that the sieve analyses changed the grain distribution by increasing the amount of fine grains. The specific gravities of the sands used were similar in the Sinop, Zonguldak, and Çine sands, while that of Trabzon sand differed due to its mineralogical properties. Internal friction angles in Sinop sand were 29.00 and 44.24, in Trabzon sand 28.05 and 38.59, in Zonguldak sand 25.51 and 39.32, and in Çine sand between 31.63 and 45.80. The minimum (e_{min}) and maximum (e_{max}) void ratios were 0.520 and 0.781 for Sinop sand, 0.600 and 0.911 for Trabzon sand, 0.555 and 0.835 for Zonguldak sand, and 0.515 and 0.927 for Çine sand. Sinop sand contains quartz, anorthite, and mica; Zonguldak sand contains anorthite and quartz; Trabzon sand contains augite, hedenbergite, anorthite, diopside, and fayalite; and Çine sand contains anorthite, anorthoclase, mica, and quartz.

Sand samples with different degrees of compaction were prepared and consolidated in a square chamber cutting experiment instrument at different vertical effective stresses. Different pressures were applied to the sands, which had been prepared in loose, tight, and medium-tight manners. Dry sand samples were used in the experiments. On the basis of the results of the experiment, a semi-empirical probabilistic model was developed that modeled the effective internal friction angle with vertical effective stress and relative compaction. It was found that the model results were generally compatible with the existing internal friction angle correlations, whereas the TRB sand, having a high specific gravity relative to the other sands, had a higher internal friction angle due to its mineral content.. Similarly, correlations were developed for slip modulus G_{25}, G_{50}, G_{75}, and G_{100} values. The results obtained from the experiments are comparable with the empirical formulas in the literature.

When the semi-empirical probabilistic slip-resistance angle relationships and semi-empirical probabilistic shift modulus relationships are examined, the error term does not show a correlation with the model input parameters D_R and Sigma, and the average error in the zero order shows the success of the obtained model in producing an objective (accurate) estimation. The elevation of the standard deviation of the model error term indicates the possible uncertainty in the calculation of the shear resistance angle based only on relative compactness and effective stress.

Acknowledgment
This study was carried out as a Post-doctoral study within the scope of the METU-DOSAP program. I would like to thank Prof. Dr. Kemal Önder ÇETİN, who contributed to the study and helped with establishment of the model.

7. References

ASTM D2487-11, Standard Practice for Classification of Soils for Engineering Purposes (Unified Soil Classification System), ASTM International, West Conshohocken, PA, 2011, www.astm.org// http://www.astm.org/Standards/D2487.htm

ASTM D 3080-98, 2003. Standart Test Method for Direct Shear of Soils Under Consolidate Drained Conditions, In: Annual Book of ASTM Standarts, Volume 04.08, Philadelphia, PA, pp. 417-422.

Bayın, 2011. Determination of residual shear strength by consolidated-drained triaxial test. Master Thesis, İstanbul, Turkey.

Bolton, M. D., 1986. The strenght and dilatancy of sand. Geotechnique 36, No. 1, 65-78.

V.F.B. de Mello, 1971, The Standard Penetration Test: Proceedings of the 4th Panamerican Conference on Soil Mechanics and Foundation Engineering: San Juan, PR, v.1:1-86

Duncan, M., 1980. Hyperbolic stress-strain relationships. Limit equilibrium,plasticity and generalized stress-strain in geotechnical engineering: Proceedings of the workshops. McGill University, May 28-30, 1980, p.443-460.

Jefferies, M.G. & Been, K. 2006. Soil Liquefaction: A critical state approach, Taylor and Francis, Abingdon, ISBN.

Ling, H. I., and Yang, S., 2006. Unified Sand Model Based on the Critical State and Generalized Plasticity. J. Eng. Mech. 2006.132:1380-1391.

Özaydın, K., 2000. Soil Mechanic. Birsen Publication. İstanbul, Turkey, s. 143-183.

Sezen, A., 2003. Micromechanism-based endochronic modeling of sand behaviour, Doctora Thesis, İstanbul, Turkey.

Sowers, G. F. (1979) "Introductory Soil Mechanics and Foundations," 4th edition. Macmillan, 621, New York

Stroud, M.A. 1989. The Standard Penetration Test – its application and interpretation. Proceedings ICE Conference on Penetration Testing in the UK, London: Thomas Telford

Şener, A., 2009. Strength of soils after earthquake shock, Master Thesis, İstanbul, Turkey.

Yüksel, B., 2007. Research of the change in the clay structures during consolidation . İstanbul, Turkey.